

Ultracold Heteronuclear Three-Body Systems: How Diabaticity Limits the Universality of Recombination into Shallow Dimers

P. Giannakeas^{1,2,*} and Chris H. Greene^{1,†}

¹*Department of Physics and Astronomy, Purdue University, West Lafayette, Indiana 47907, USA*

²*Max Planck Institute for the Physics of Complex Systems, Nöthnitzer Straße 38, 01187 Dresden, Germany*



(Received 30 June 2017; published 12 January 2018)

The mass-imbalanced three-body recombination process that forms a shallow dimer is shown to possess a rich Efimov-Stückelberg landscape, with corresponding spectra that differ fundamentally from the homonuclear case. A semianalytical treatment of the three-body recombination predicts unusual spectra with intertwined resonance peaks and minima and yields in-depth insight into the behavior of the corresponding Efimov spectra. In particular, the patterns of the Efimov-Stückelberg landscape are shown to depend inherently on the degree of diabaticity of the three-body collisions, which strongly affects the universality of the heteronuclear Efimov states.

DOI: [10.1103/PhysRevLett.120.023401](https://doi.org/10.1103/PhysRevLett.120.023401)

The infinite geometric progression of trimer states, even when all the two-body subsystems are barely unbound, consists of the most counterintuitive few-body phenomenon, namely, the Efimov effect [1,2]. The exotic Efimov states have received extensive theoretical and experimental study [3–11] addressing the underlying physical principles, such as the universality of the ground Efimov state [12–19] and the discrete scaling invariance for successive Efimov states for homonuclear [20] and heteronuclear systems, i.e., heavy-heavy-light (HHL) [21–23]. Recent experimental evidence on mass-imbalanced ensembles suggests that the Efimov spectra possess a far richer landscape than the homonuclear counterparts [24–26] stemming from the large parameter space.

HHL systems possess two scattering lengths, i.e., a_{HH} and a_{HL} , which define four main categories of behavior according to the signs alone, since each a_{ij} can be positive or negative. Additional subcategories unfold depending on the magnitude, i.e., $|a_{\text{HH}}|/|a_{\text{HL}}| \gtrsim 1$. Spanning a large portion of parameter space, Refs. [21,22,25,27,28] experimentally and theoretically explored the three-body losses of the ${}^6\text{Li}$ – ${}^{133}\text{Cs}$ – ${}^{133}\text{Cs}$ system, demonstrating that the different signs in the intraspecies scattering lengths ($a_{\text{CsCs}} \gtrsim 0$) render an inherently different Efimovian landscape. Additional experimental efforts for the case $a_{\text{HH}} > 0$ illustrate deviations of the universal theory from the observed Efimov spectra [26] in the regime where the two-body interspecies interactions; i.e., a_{HL} are tuned via narrow Fano-Feshbach resonances [29]. These investigations pose the most intriguing questions in the few-body physics of HHL systems: whether the three-body physics is universal, whether the Efimov spectrum needs a nonuniversal “three-body parameter” (3BP) to specify its lowest state, and whether van der Waals (vdW) physics approximately determines that 3BP, as experimental and

theoretical evidence suggests is true for the homonuclear case [13,14,16–18,30]. Therefore, a more flexible and complete theoretical description of three-body recombination (3BR) into shallow dimers ($a_{\text{HH}} > 0$) is needed.

This Letter develops a semiclassical theoretical treatment based on the adiabatic hyperspherical representation with nonadiabatic coupling included addressing shallow dimer recombination for HHL systems. We demonstrate that the universality for various observables in this system is strongly affected by the degree of diabaticity connecting the three-body continuum and recombination channels. Adiabatic collisions exhibit the Efimov physics idiosyncrasies which depend *only* on the scattering lengths, rendering the three-body system *fully* universal. In contrast to the homonuclear case, heteronuclear systems with positive intraspecies and negative interspecies interactions (i.e., $a_{\text{HH}} > 0$ and $a_{\text{HL}} < 0$, respectively) exhibit 3BR rates whose landscape for varying scattering lengths was previously predicted [31] to consist of Efimov resonances intertwined with a series of Stückelberg interference minima [32,33]. The present analysis shows how the assumption of hyperradial adiabaticity underlying the original prediction by D’Incao and Esry [31] must be generalized when the relevant Landau-Zener transition probability is closer to diabatic than adiabatic, as is true for strong mass-imbalanced systems.

Our prototype three-body system consists of two heavy (H) atoms and a light (L) one, which collide at low energies via *s*-wave zero-range interactions. The 3BR into a shallow heavy-heavy (HH) dimer and a recoiling light atom is achieved by considering the intraspecies (interspecies) interactions to possess a positive (negative) scattering length, i.e., $a_{\text{HH}} > 0$ ($a_{\text{HL}} < 0$). The paraphernalia of the adiabatic hyperspherical representation (for a detailed review, see Ref. [11]) is employed in the following addressing the three-body physics of interest. In this representation,

the properly symmetrized total wave function is written as $\Psi(R, \Omega) = R^{-5/2} \sum_{\nu} \phi_{\nu}(R; \Omega) F_{\nu}(R)$, where $\phi_{\nu}(R; \Omega)$ [$F_{\nu}(R)$] refers to the ν th hyperangular [hyperradial] component of $\Psi(R, \Omega)$. The hyperangular factor is an eigenfunction of the fixed- R adiabatic equation [34]:

$$H_{\text{ad}}(R; \Omega) \phi_{\nu}(R; \Omega) = U_{\nu}(R) \phi_{\nu}(R; \Omega), \quad (1)$$

where Ω collectively denotes the five hyperangles whereas R is the hyperradius [35,36]. The $U_{\nu}(R)$ are the adiabatic hyperspherical potential curves, and H_{ad} contains the hyperangular kinetic operator together with the pairwise zero-range interactions. After integrating over all the hyperangles Ω , the three-body Schrödinger equation reads

$$\left(-\frac{d^2}{dR^2} + \frac{2\mu}{\hbar^2} (U_{\nu} - E) \right) F_{\nu}(R) = \sum_{\nu'} V_{\nu\nu'} F_{\nu'}(R), \quad (2)$$

where $\mu = m_{\text{H}} / \sqrt{1 + 2m_{\text{H}}/m_{\text{L}}}$ is the three-body reduced mass, m_{H} (m_{L}) denotes the mass of the heavy (light) atom, and E indicates the total relative energy. $V_{\nu\nu'} = 2P_{\nu\nu'}(R)(d/dR) + Q_{\nu\nu'}(R)$ are the R -dependent nonadiabatic coupling matrix elements obeying the relations $P_{\nu\nu'} = \langle \phi_{\nu}(R; \Omega) | (\partial/\partial R) \phi_{\nu'}(R; \Omega) \rangle_{\Omega}$ and $Q_{\nu\nu'} = \langle \phi_{\nu}(R; \Omega) | (\partial^2/\partial R^2) \phi_{\nu'}(R; \Omega) \rangle_{\Omega}$. Note that the symbol $\langle \dots \rangle_{\Omega}$ indicates the integration over the hyperangles *only*. For zero-range interactions, U_{ν} , $P_{\nu\nu'}$, and $Q_{\nu\nu'}$ are known semianalytically [3,37–39].

Figure 1(a) illustrates within the two-channel approximation the physical picture of a shallow dimer recombination process with $a_{\text{HH}} > 0$ and $a_{\text{HL}} < 0$. In Fig. 1(a), the first two adiabatic potential curves $U_{\nu}^{1/3}(R)$ (solid blue and

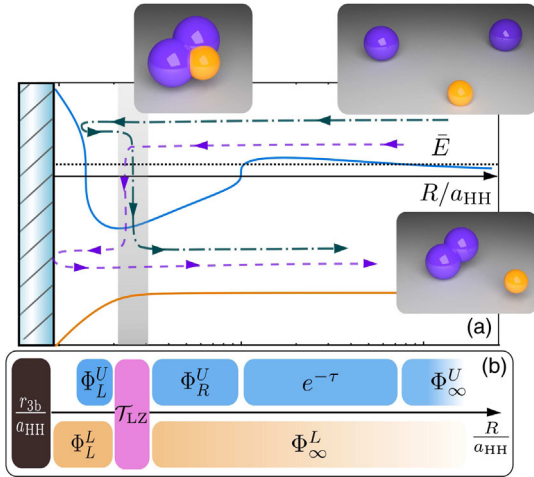


FIG. 1. (a) The two lowest hyperspherical potential curves $U_{\nu}^{1/3}(R/a_{\text{HH}})$ (orange and blue solid curves) for a HHL system with mass ratio $m_{\text{H}}/m_{\text{L}} = 22.1$, $a_{\text{HL}} < 0$, $a_{\text{HH}} > 0$, and the total energy \bar{E} in units of $\hbar^2/m_{\text{H}}a_{\text{HH}}^2$ is indicated as a black dotted line. The blue hatched area indicates the 3BP at $R = r_{3\text{b}}$, whereas the gray region depicts the maximum of the P -matrix. The green dash-dotted and purple dashed lines denote the dominant two interfering pathways. (b) An illustration of the terms associated with the semiclassical treatment and their connections to the curves shown in (a).

orange lines) are depicted as functions of the scaled hyperradius R/a_{HH} . The mass ratio between the heavy and light particle is set $m_{\text{H}}/m_{\text{L}} = 22.1$ corresponding to ${}^6\text{Li}-{}^{133}\text{Cs}-{}^{133}\text{Cs}$ collisions. The 3BP is introduced as a hard wall boundary condition at $R = r_{3\text{b}}$ [see the blue hatched area in Fig. 1(a)], avoiding the Thomas collapse [40]. The gray box in Fig. 1(a) indicates the hyperradial region where the nonadiabatic coupling P -matrix element maximizes, namely, the nonadiabatic transition region. At the indicated total relative energy \bar{E} , written in units of $\hbar^2/m_{\text{H}}a_{\text{HH}}^2$ [see the dotted line in Fig. 1(a)] and $R/a_{\text{HH}} \rightarrow \infty$, the three particles are asymptotically free. But as R/a_{HH} decreases, the system tunnels inward under the barrier probing the classically allowed region of the upper potential curve (blue solid line). Because of the nonadiabatic coupling (see the gray box), the three particles can recombine to the lower potential curve (orange solid line), forming a shallow HH dimer and a recoiling light particle. To quantitatively address this physical process, a fully semiclassical treatment of Eq. (2) is developed within the two-channel approximation, yielding an analytical expression for the corresponding 3BR rate K_3 :

$$K_3 = \frac{64\hbar\pi^2}{\mu k^4} |S_{12}|^2, \quad \text{with} \quad |S_{12}|^2 = e^{-2\tau} p(1-p) \frac{N}{D},$$

$$N = \cos^2 \left(\Phi_L^U - \Phi_L^L - \frac{\pi}{4} + \lambda \right),$$

$$D = \left(1 - \frac{e^{-4\tau}}{16} \right) \left[p \cos^2 \left(\Phi_L^L + \Phi_R^U - \frac{\pi}{4} \right) + (1-p) \cos^2 \left(\Phi_L^U + \Phi_R^U + \lambda \right) \right]$$

$$- \left(1 - \frac{e^{-2\tau}}{4} \right)^2 p(1-p) N + \frac{e^{-4\tau}}{16}. \quad (3)$$

Here $k^2 = 2\mu E/\hbar^2$, and $|S_{12}|^2$ denotes the S -matrix element describing the 3BR into a universal shallow dimer. Figure 1(b) depicts the terms that appear in Eq. (3). The terms Φ_{α}^i with $i = L, U$ and $\alpha = L, R$ indicate the Jeffreys-Wentzel-Kramers-Brillouin phases (including the Langer correction [32]) of the upper ($i = U$) and lower ($i = L$) potential curves of Fig. 1(a) on the left- ($\alpha = L$) and right-hand side ($\alpha = R$) of the transition region, i.e., the gray box in Fig. 1(a). The asymptotic phases of the upper and lower curves are indicated by Φ_{∞}^U and Φ_{∞}^L , respectively, and, of course, the $|S_{12}|^2$ does not depend on them. Note that Φ_{∞}^U is defined from the outer classical turning point of the upper Efimov curve, whereas Φ_{∞}^L is defined from hyperradii beyond the nonadiabatic transition region. In Fig. 1(b), the factor $e^{-\tau}$ indicates the tunneling amplitude in the classically forbidden region of the upper potential curve [see the blue solid line in Fig. 1(a)]. The 3BP is indicated in Fig. 1(b) by the far left black box.

The phase λ and the term p in Eq. (3) as well as the term \mathcal{T}_{LZ} in Fig. 1(b) are associated with the Landau-Zener physics [41]. p indicates the nonadiabatic transition probability from the upper to the lower potential curve shown in

Fig. 1(a) which is evaluated by the P -matrix elements [42]. The phase λ is associated with the pass of the hyperradial wave function through the nonadiabatic transition region and solely depends on the probability p [43,44]. This nontrivial phase is necessary for an accurate 3BR coefficient, as our numerical tests suggest. The $\mathcal{T}_{LZ} \equiv \mathcal{T}_{LZ}(\lambda, p)$ denotes the nonadiabatic transition matrix which interrelates the adiabatic hyperradial wave function bilaterally of the transition region as shown in Fig. 1(a) [43,44].

The analytical expression of K_3 in Eq. (3) conveys the most important attributes of a recombination process into a shallow HH dimer for the HHL system. The key role is played here by the degree of diabaticity, namely, the nonadiabatic probability p in K_3 , and inherently modifies the properties of the Efimov spectra, whereas in the homonuclear cases the corresponding p is trivially an overall prefactor in K_3 . The resonant enhancement of K_3 mainly arises due to the resonant denominator D in Eq. (3), which explicitly depends on the nonadiabatic transition probability p . Hence, the Efimov spectra are influenced by the degree of diabaticity of the three-body collisions. For example, in mostly diabatic collisions, i.e., $p \approx 1$, the Efimov resonances in K_3 depend on the phase Φ_L^L , which is defined by the 3BP [see Fig. 1(b)]. For adiabatic three-body collisions, i.e., $p \approx 0$, K_3 is virtually independent of the Φ_L^L phase. Therefore, a mostly adiabatic 3BR process possesses a fully universal Efimov spectrum which is independent of any 3BP. This adiabatic limit was stressed in the case of vdW two-body interactions study presented by Refs. [24,25]. The probability p , in general, depends mainly on the $|a_{HL}|/a_{HH}$ and the mass ratio $\beta = (m_H/m_L)$, but, in principle, it could be affected by the vdW physics in realistic scenarios. In Fig. 2(d), p varies monotonically in the interval (0.55,0.87) for $|a_{HL}|/a_{HH} \in (4.2, 123.4)$, respectively, matching the regime of Refs. [24–26] around $B = 889$ G. In the unitarity limit ($|a_{HL}|/a_{HH} \rightarrow \infty$), p obeys the fitting relation $p_\infty \sim e^{-[16/(2\beta+1)]+0.22}$ for $2.3 < \beta < 23$ to a good approximation. The latter implies that large mass ratios yield mostly diabatic 3BR processes.

Equation (3) exhibits also signatures of Stückelberg physics. The numerator of $|S_{12}|^2$ depends on the phases Φ_L^U and Φ_L^L emerging from a two-pathway interference [see the green dash-dotted and purple dashed lines in Fig. 1(a)] and can cause a suppression of K_3 , i.e., Stückelberg minima, which is nonuniversal due to the Φ_L^L phase. Note that the semiclassical theory developed here for K_3 in Eq. (3) generalizes and extends the study by Ref. [31], through our inclusion of the explicit dependence on the nonadiabatic probability p . This analysis also provides a systematic pathway to generalize Eq. (3) to positive inter- and intraspecies interactions going beyond previous studies [45,46].

Our calculated 3BR coefficient is illustrated in Fig. 2, where the system of ${}^6\text{Li}-{}^{133}\text{Cs}-{}^{133}\text{Cs}$ is considered. Figure 2 depicts the scaled 3BR coefficient $m_{\text{Cs}}K_3/\hbar a_{\text{LiCs}}^4$ at low energies \bar{E} (in units of $\hbar^2/m_H a_{\text{HH}}^2$), as a function of the ratios r_{3b}/a_{CsCs}

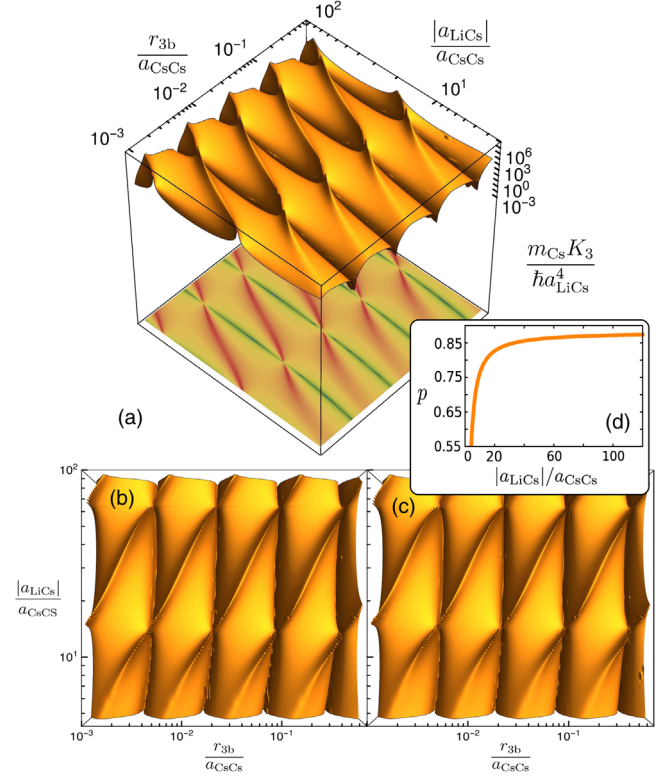


FIG. 2. The scaled 3BR coefficient $m_{\text{Cs}}K_3/\hbar a_{\text{LiCs}}^4$ at low energy \bar{E} (in units of $\hbar^2/m_H a_{\text{HH}}^2$) for the ${}^6\text{Li}-{}^{133}\text{Cs}-{}^{133}\text{Cs}$ system as a function of two ratios: the 3BP r_{3b}/a_{CsCs} and the interspecies scattering length $|a_{\text{LiCs}}|/a_{\text{CsCs}}$. Panels (b) and (c) show the scaled 3BR calculations within the semiclassical treatment and the R -matrix numerical simulations, respectively. Panel (d) depicts the probability p versus $|a_{\text{LiCs}}|/a_{\text{CsCs}}$.

and $|a_{\text{LiCs}}|/a_{\text{CsCs}}$. Figure 2(a) refers to a direct numerical solution of Eq. (2) within the two-channel approximation using the R -matrix propagation method (for details, see Refs. [47,48]). Figure 2(a) conveys the rich structure that arises in the 3BR coefficient. The enhancements in $m_{\text{Cs}}K_3/\hbar a_{\text{LiCs}}^4$ emerge from metastable Efimov states that resonantly transfer probability flux from the three-body continuum into the atom-dimer continuum via the nonadiabatic region [see the red stripes in the contour plot in Fig. 2(a)]. Within the zero-range approximation, the position of the Efimov resonances $m_{\text{Cs}}K_3/\hbar a_{\text{LiCs}}^4$ depend on the 3BP, i.e., (r_{3b}/a_{CsCs}), since for this system the three-body collision is closer to being a diabatic process. $m_{\text{Cs}}K_3/\hbar a_{\text{LiCs}}^4$ also exhibits Stückelberg minima [see the green stripes in the contour plot in Fig. 2(a)] which are virtually insensitive to variations of the ratio $|a_{\text{LiCs}}|/a_{\text{CsCs}}$. This feature of coexisting Efimov resonances and Stückelberg minima is inherent in HHL systems with $a_{\text{HL}} < 0$ and $a_{\text{HH}} > 0$. In contrast, for homonuclear recombination processes that produce a shallow dimer, at positive scattering lengths one observes only Stückelberg minima.

In the ${}^6\text{Li}-{}^{133}\text{Cs}-{}^{133}\text{Cs}$ system, the Stückelberg minima persist even at $|a_{\text{LiCs}}|/a_{\text{CsCs}} < 4$. The latter corresponds to

magnetic fields $891 \leq B \leq 950$ G, where the ratio $|a_{\text{LiCs}}|/a_{\text{CsCs}} \in (4.27, 0.05)$ and $a_{\text{CsCs}} \in (227a_0, 991a_0)$ provide enough parameter tunability in order to experimentally probe the Stückelberg minima. From Ref. [49], the 3BR rates are suppressed for Cs atoms at $B = 893$ G. Additional Stückelberg physics in the Li–Cs₂ channel might enable the production of a gas of two bosonic species that keeps high densities throughout a cooling process as was also discussed in Ref. [50].

Figures 2(b) and 2(c) compare the scaled 3BR rates calculated with Eq. (3) and with the R -matrix theory, respectively, showing good agreement. Figures 2(b) and 2(c) exhibit two different log-periodic scaling behaviors versus the axis of r_{3b}/a_{CsCs} and $|a_{\text{LiCs}}|/a_{\text{CsCs}}$, a distinct feature of the Efimov physics in this system.

In the spirit of Ref. [51], the $|S_{12}|^2$ matrix elements in Eq. (3) can be further approximated, focusing thus on the diabaticity and log-periodicity of the K_3 . When E is the lowest energy scale in the system, the upper and lower adiabatic potential curves illustrated in Fig. 1(a) can be parametrized as $U_1(R) = -(\hbar^2/2\mu R^2)(s_0^2 + 1/4)$ (for $a_{\text{HH}} \ll R \ll |a_{\text{HL}}|$) and $U_2(R) = -(\hbar^2/2\mu R^2)[(s_0^*)^2 + 1/4]$ (for $R \ll a_{\text{HH}} \ll |a_{\text{HL}}|$), respectively. As in Ref. [52], s_0 (s_0^*) corresponds to a universal Efimov scaling coefficient for two (three) resonant interactions. Then $|S_{12}|^2$ simplifies to

$$\frac{|S_{12}|^2}{(ka_{\text{HL}})^4} = \frac{p(1-p)\cos^2(s_0^* \ln \frac{r_{3b}}{a_{\text{HH}}} + \psi_1)}{\mathcal{P}(\frac{r_{3b}}{a_{\text{HH}}}, \frac{|a_{\text{HL}}|}{a_{\text{HH}}})}, \quad (4)$$

where $\mathcal{P}(r_{3b}/a_{\text{HH}}, |a_{\text{HL}}|/a_{\text{HH}}) = p \sin^2[s_0 \ln(|a_{\text{HL}}|/a_{\text{HH}}) + \psi_2 - (s_0^* \ln(r_{3b}/a_{\text{HH}}) + \psi_1)] + (1-p)\cos^2(s_0 \times \ln(|a_{\text{HL}}|/a_{\text{HH}}) + \psi_2) - p(1-p)\cos^2(s_0^* \ln(r_{3b}/a_{\text{HH}}) + \psi_1)$. ψ_1 and ψ_2 are arbitrary constant phases and are treated as fitting parameters. Note that Eq. (4) is valid for $|a_{\text{HL}}| \gg a_{\text{HH}} \gg r_{3b}$. Elegantly, Eq. (4) shows that $|S_{12}|^2$ depends on two geometric scalings where s_0^* (s_0) solely determines the Stückelberg minima (Efimov resonances). Note that, in the limit of large mass ratio, $s_0^* \approx s_0$. Figures 3(a)–3(c) illustrate the effects of diabaticity in (K_3/a_{HL}^4) using Eq. (4) within two successive Stückelberg minima where the nonadiabatic probability p is parametrically adjusted; i.e., Figs. 3(a)–3(c) correspond to $p = (0.8, 0.4, 0.1)$, respectively. Note that the universal scaling factors s_0 and s_0^* are taken from Ref. [52] for the physical system of ${}^6\text{Li}$ – ${}^{133}\text{Cs}$ – ${}^{133}\text{Cs}$, whereas the phases ψ_1 and ψ_2 are arbitrarily chosen. Evidently, Figs. 3(a)–3(c) unravel the universal aspects of the Efimov resonances in terms of the degree of diabaticity. Figure 3(a) depicts the predominantly diabatic regime ($p = 0.8$) where the positions of the Efimov resonances strongly depend on the ratio r_{3b}/a_{CsCs} , namely, on the 3BP. Notice that the trajectories of the resonant enhancements, namely, Efimov manifolds, shift upwards as r_{3b}/a_{CsCs} increases. Intuitively, this effect is best understood in the diabatic picture [see Fig. 3(d)], where the “diabatized” hyperspherical curves are shown,

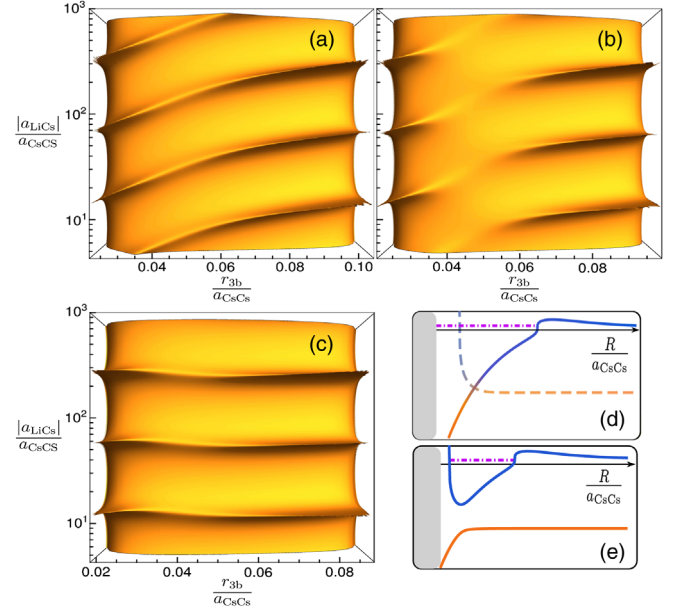


FIG. 3. The scaled 3BR $m_{\text{Cs}}K_3/\hbar a_{\text{LiCs}}^4$ at $\bar{E} \rightarrow 0$ for ${}^6\text{Li}$ – ${}^{133}\text{Cs}$ – ${}^{133}\text{Cs}$ using Eq. (4). Panels (a)–(c) correspond to different nonadiabatic probabilities, namely, $p = (0.8, 0.4, 0.1)$, respectively. Panels (d) and (e) present schematic illustrations of the diabatic and adiabatic hyperspherical potentials, respectively. The magenta dash-dotted line indicates the quasibound Efimov state, and the gray box depicts the 3BP.

whereas the magenta dash-dotted line indicates the Efimov metastable state. The diabatic potential curve (solid line) which supports the Efimov states depends on the 3BP (gray box). Therefore, the energy of an Efimov quasibound state remains in resonance only by simultaneously increasing the 3BP and the $|a_{\text{HL}}|/a_{\text{HH}}$. Note that the maximum of the potential barrier in Fig. 3(e) increases as $R_b \sim 0.34|a_{\text{HL}}|m_{\text{H}}/\mu$.

Interestingly, in the adiabatic limit, shown in Fig. 3(c) for $p = 0.1$, the Efimov resonance manifolds acquire universal characteristics and become virtually independent of the 3BP. This attribute can be understood by inspecting the potential curves in Fig. 3(e) showing the adiabatic version of the potential curves. Figure 3(c) shows that the 3BP only weakly affects the Efimov quasibound states (see the magenta dash-dotted line) due to the repulsive barrier at a small hyperradius (see the blue solid line) which shields the three particles from exploring the nonuniversal region that depends on the 3BP.

In the diabatic-to-adiabatic regime [see Fig. 3(b)] [$p = (0.4)$], the Efimov manifolds undergo a rearrangement where at $r_{3b}/a_{\text{CsCs}} \approx 0.05$ each manifold is “interrupted” and for $p = 0.1$ [see Fig. 3(c)] is “reattached” with the next one. This effect is mainly related to the widths of the Efimov resonances with respect to r_{3b}/a_{CsCs} . Particularly, in all the panels in Fig. 3, the Efimov manifolds are broader at $r_{3b}/a_{\text{CsCs}} \approx 0.05$, whereas close to the Stückelberg minima they become narrower. This

dependence of the width of the Efimov resonances on the 3BP can be understood in terms of the two dominant interfering paths for the recombination into a shallow dimer [see the dashed and dot-dashed lines in Fig. 1(a)]. Close to the Stückelberg minima due to the destructive interference of the two pathways, the Efimov quasibound state is weakly coupled to the atom-dimer continuum, yielding a narrow Efimov manifold. But for $r_{3b}/a_{CsCs} \approx 0.05$ the two pathways interfere constructively; hence, the trimer metastable state is strongly coupled to the continuum broadening the Efimov manifolds. Figure 3(b) demonstrates that for $p = 0.4$ the two pathways interfere maximally, yielding maximally broad Efimov manifolds that are completely smeared out by the atom-dimer continuum.

Conclusions.—The detailed idiosyncrasies of the Efimov physics for mass-imbalanced ultracold systems are investigated, with a focus on recombination processes into shallow HH dimer states. Our semiclassical analysis is based on the adiabatic hyperspherical representation including the Landau-Zener physics, yielding a closed-form expression for the corresponding 3BR rate. A rich Efimov–Stückelberg landscape is illustrated from our analysis as a unique feature of the mass-imbalanced systems where the degree of diabaticity constrains the Efimovian universality. Namely, a diabatic recombination processes depends strongly on the 3BP. In the diabatic-to-adiabatic regime, the Efimov state manifolds exhibit a rearrangement effect and illustrate the transition from system-dependent Efimov resonances to system-independent ones. The present development can be generalized to include vdW two-body interactions in order to elucidate the extent to which the 3BP is constrained beyond the zero-range theories.

The authors thank P. S. Julienne, S. T. Rittenhouse, N. P. Mehta, and M. T. Eiles for fruitful discussions and acknowledge the Max Planck Institute for the Physics of Complex Systems in Dresden for the warm hospitality and partial financial support. This work was supported in part by National Science Foundation (NSF) Grant No. PHY-1607180. The numerical calculations were performed under NSF XSEDE Resource Allocation No. TG-PHY150003.

*pgiannak@purdue.edu

†chgreene@purdue.edu

- [1] V. Efimov, *Phys. Lett. B* **33**, 563 (1970).
- [2] T. Kraemer, M. Mark, P. Waldburger, J. G. Danzl, C. Chin, B. Engeser, A. D. Lange, K. Pilch, A. Jaakkola, H. C. Nägerl, and R. Grimm, *Nature (London)* **440**, 315 (2006).
- [3] E. Nielsen, D. V. Fedorov, A. S. Jensen, and E. Garrido, *Phys. Rep.* **347**, 373 (2001).
- [4] K. Riisager, *Rev. Mod. Phys.* **66**, 1105 (1994).
- [5] E. Braaten and H. W. Hammer, *Phys. Rep.* **428**, 259 (2006).
- [6] S. T. Rittenhouse, J. von Stecher, J. D’Incao, N. Mehta, and C. H. Greene, *J. Phys. B* **44**, 172001 (2011).
- [7] D. Blume, *Rep. Prog. Phys.* **75**, 046401 (2012).
- [8] Y. Wang, J. P. D’Incao, and B. D. Esry, *Ultracold Few-Body Systems*, in *Advances In Atomic, Molecular, and Optical Physics*, Vol. 62, (Academic Press, New York, 2013), pp. 1–115.
- [9] Y. Wang, P. Julienne, and C. H. Greene, in *Annual Review of Cold Atoms and Molecules*, Vol. 3, edited by K. W. Madison, K. Bongs, L. D. Carr, A. M. Rey, and H. Zhai (World Scientific, Singapore, 2015), pp. 77–134.
- [10] P. Naidon and S. Endo, *Rep. Prog. Phys.* **80**, 056001 (2017).
- [11] C. H. Greene, P. Giannakeas, and J. Pérez-Ríos, *Rev. Mod. Phys.* **89**, 035006 (2017).
- [12] Y. Wang and P. S. Julienne, *Nat. Phys.* **10**, 768 (2014).
- [13] S. Roy, M. Landini, A. Trenkwalder, G. Semeghini, G. Spagnolli, A. Simoni, M. Fattori, M. Inguscio, and G. Modugno, *Phys. Rev. Lett.* **111**, 053202 (2013).
- [14] J. Wang, J. P. D’Incao, B. D. Esry, and C. H. Greene, *Phys. Rev. Lett.* **108**, 263001 (2012).
- [15] N. Gross, Z. Shotan, S. Kokkelmans, and L. Khaykovich, *Phys. Rev. Lett.* **103**, 163202 (2009).
- [16] P. Naidon, S. Endo, and M. Ueda, *Phys. Rev. Lett.* **112**, 105301 (2014).
- [17] P. Naidon, S. Endo, and M. Ueda, *Phys. Rev. A* **90**, 022106 (2014).
- [18] F. Ferlaino and R. Grimm, *Physics* **3**, 9 (2010).
- [19] M. Kunitski, S. Zeller, J. Voigtsberger, A. Kalinin, L. P. H. Schmidt, M. Schoeffler, A. Czasch, W. Schoellkopf, R. E. Grisenti, T. Jahnke, D. Blume, and R. Doerner, *Science* **348**, 551 (2015).
- [20] B. Huang, L. A. Sidorenkov, R. Grimm, and J. M. Hutson, *Phys. Rev. Lett.* **112**, 190401 (2014).
- [21] R. Pires, J. Ulmanis, S. Häfner, M. Repp, A. Arias, E. D. Kuhnle, and M. Weidemüller, *Phys. Rev. Lett.* **112**, 250404 (2014).
- [22] J. Ulmanis, S. Häfner, R. Pires, E. D. Kuhnle, M. Weidemüller, and E. Tiemann, *New J. Phys.* **17**, 055009 (2015).
- [23] S. K. Tung, K. Jimenez-Garcia, J. Johansen, C. V. Parker, and C. Chin, *Phys. Rev. Lett.* **113**, 240402 (2014).
- [24] J. Ulmanis, S. Häfner, R. Pires, E. D. Kuhnle, Y. Wang, C. H. Greene, and M. Weidemüller, *Phys. Rev. Lett.* **117**, 153201 (2016).
- [25] S. Häfner, J. Ulmanis, E. D. Kuhnle, Y. Wang, C. H. Greene, and M. Weidemüller, *Phys. Rev. A* **95**, 062708 (2017).
- [26] J. Johansen, B. J. DeSalvo, K. Patel, and C. Chin, *Nat. Phys.* **13**, 731 (2017).
- [27] D. S. Petrov and F. Werner, *Phys. Rev. A* **92**, 022704 (2015).
- [28] M. Mikkelsen, A. S. Jensen, D. V. Fedorov, and N. T. Zinner, *J. Phys. B* **48**, 085301 (2015).
- [29] C. Chin, R. Grimm, P. Julienne, and E. Tiesinga, *Rev. Mod. Phys.* **82**, 1225 (2010).
- [30] N. Gross, Z. Shotan, S. Kokkelmans, and L. Khaykovich, *Phys. Rev. Lett.* **103**, 163202 (2009).
- [31] J. P. D’Incao and B. D. Esry, *Phys. Rev. Lett.* **103**, 083202 (2009).
- [32] E. Nielsen and J. H. Macek, *Phys. Rev. Lett.* **83**, 1566 (1999).
- [33] B. D. Esry, C. H. Greene, and J. P. Burke Jr., *Phys. Rev. Lett.* **83**, 1751 (1999).
- [34] H. Suno, B. Esry, and C. H. Greene, *New J. Phys.* **5**, 53 (2003).

- [35] J. Avery, *Hyperspherical Harmonics: Applications in Quantum Theory* (Kluwer Academic, Norwell, MA, 1989).
- [36] Y. F. Smirnov and K. V. Shitikova, *Sov. J. Part. Nucl.* **8**, 44 (1977).
- [37] S. T. Rittenhouse, N. P. Mehta, and C. H. Greene, *Phys. Rev. A* **82**, 022706 (2010).
- [38] O. I. Kartavtsev and A. V. Malykh, *J. Phys. B* **40**, 1429 (2007).
- [39] O. I. Kartavtsev and A. V. Malykh, *Phys. Rev. A* **74**, 042506 (2006).
- [40] L. H. Thomas, *Phys. Rev.* **47**, 903 (1935).
- [41] The explicit forms of \mathcal{T}_{LZ} and λ are given in Eqs. (19), (20), and (23) in Ref. [43].
- [42] C. W. Clark, *Phys. Lett. A* **70**, 295 (1979).
- [43] M. Child, *J. Mol. Spectrosc.* **53**, 280 (1974).
- [44] C. Zhu and H. Nakamura, *J. Chem. Phys.* **101**, 10630 (1994).
- [45] K. Helfrich, H.-W. Hammer, and D. S. Petrov, *Phys. Rev. A* **81**, 042715 (2010).
- [46] B. Acharya, C. Ji, and L. Platter, *Phys. Rev. A* **94**, 032702 (2016).
- [47] N. P. Mehta, B. D. Esry, and C. H. Greene, *Phys. Rev. A* **76**, 022711 (2007).
- [48] J. P. Burke Jr., Ph.D. thesis, University of Colorado, 1999.
- [49] M. Berninger, A. Zenesini, B. Huang, W. Harm, H.-C. Nägerl, F. Ferlaino, R. Grimm, P. S. Julienne, and J. M. Hutson, *Phys. Rev. Lett.* **107**, 120401 (2011).
- [50] M. Repp, R. Pires, J. Ulmanis, R. Heck, E. D. Kuhnle, M. Weidemüller, and E. Tiemann, *Phys. Rev. A* **87**, 010701 (2013).
- [51] J. P. D'Incao and B. D. Esry, *Phys. Rev. Lett.* **94**, 213201 (2005).
- [52] Y. Wang, J. Wang, J. P. D'Incao, and C. H. Greene, *Phys. Rev. Lett.* **109**, 243201 (2012).